LAWRENCE
LIVERMORE
NATIONAL
LABORATORY

UCRL-JRNL-219993

A viscoplastic micromechanical model for the yield strength of nanocrystalline materials

R. Lebensohn, E. Bringa, A. Caro

March 22, 2006

Acta Materialia

A viscoplastic micromechanical model for the yield strength of nanocrystalline materials

R.A. Lebensohn (*), E.M Bringa (**) and A. Caro (**)

(*) Los Alamos National Laboratory, NM 87545, USA
(**) Lawrence Livermore National Laboratory, CA 94550, USA

ABSTRACT

In this paper we present a micromechanical approach based on Fast Fourier Transforms to study the role played by dislocation glide and grain boundary (GB) accommodation in the determination of the plastic behavior of nanostructured materials. For this, we construct unit cells representing self-similar polycrystals with different grain sizes in the nanometer range and use local constitutive equations for slip and GB accommodation. We study the effect of grain size, strain rate and pressure on the local and effective behavior of nanostructured fcc materials with parameters obtained from experiments and atomistic simulations. Predictions of a previous qualitative pressure-sensitive model for the effective yield strength behind a shock front are substantially improved by considering strain partition between slip and GB activity. Under quasiestatic conditions, assuming diffusion-controlled mechanisms at GB, the model predicts a strain-rate sensitivity increase in nanocrystalline samples with respect to the same coarse-grained material of the same order as in recently published experiments.

KEYWORDS: nanocrystalline materials, micromechanical modelling, grain boundary, plastic deformation, shock loading.

1- INTRODUCTION

The yield strength of polycrystalline materials depends strongly on their grain size. For aggregates with grains in the micron range and above, the yield stress increases inversely with the square root of the grain size. This dependence, known as Hall-Petch effect [1,2] has been explained in terms of dislocation interaction with the crystal lattice, with other dislocations, and with grain boundaries (GBs). For coarse-grained (CG) aggregates, the GBs main role is to act as barriers to dislocation motion and promote the formation of pile-ups in the bulk of the grains, (e.g. [3]). Smaller grains require higher stress to move a dislocation through the stress field created by the pile-ups. In spite of the importance that this barrier effect has in the determination of the mechanical properties of the aggregate, in polycrystals with grains in the micron range and above, the highly disordered GB regions represent only a negligible volume fraction of the material. On the contrary, when the grain dimensions approach nanometer sizes, the volume fraction of GBs become significant. Then, the GB regions start to play an active role in accommodating deformation [3-10], not only at very low deformation rates when diffusional flow at GBs becomes significant regardless of the grain size, but at any applied strain rate. This GB accommodation may involve local shear shuffling of atoms, GB sliding, and/or diffusive processes that happen near the GBs. Regardless of the specific atomic displacements involved in GB accommodation, given the highly disordered character of the GB regions, the microscopic mechanisms associated with GB activity are intrinsically different from the ones associated with plastic deformation by dislocation motion that takes place in the bulk of the grains. GB accommodation has similarities with the plasticity of metallic glasses or of granular media, i.e. sliding of non-deformable objects controlled by friction [9]. Therefore, a sound constitutive equation of GB deformation would not involve directionality, as it is indeed the case of the usual constitutive description of crystal plasticity. Also, due to the short range of the interactions involved in GB accommodation, the stress required to activate this mechanism should be essentially independent of the grain size of the aggregate [11]. Furthermore, the constitutive equations that describe dislocation glide in the bulk of the grains and accommodation at GBs will have, in general, different sensitivities to temperature, strain rate and pressure. Given the role

played by diffusion at grain boundaries, the sensitivities of GB accommodation to temperature and strain rate under quasiestatic loading conditions, should be in general higher than the corresponding sensitivities associated with dislocation slip. This determines a faster decrease in yield strength with increasing temperature [12,13] and decreasing strain rate [12-17], as the grain size decreases. Regarding pressure sensitivity, given that both GB accommodation [9-11] and dislocation glide (e.g. [18]) are likely to become more difficult as hydrostatic pressure increases, the overall effect of pressure on plastic deformation of materials with nano-sized grains is going to be determined by the relative values of the corresponding sensitivity factors. A constitutive micromechanical model incorporating such sensitivities would be able to capture the interplay and competition between bulk and GB mechanisms for a particular topology of these nanostructured aggregates. Such a model could be used as a predictive tool to obtain the mechanical behavior of the aggregate, and its sensitivity to different deformation conditions and/or microstructural changes.

In conjunction with the growing interest in an accurate characterization of the mechanical behavior of nanostructured materials through an intensive experimental research, several attempts to construct models of the above kind have been recently published. Using crystallographic elasto-viscoplastic Finite Element analysis, Fu et al [19, 20] investigated different assumptions for the strain-hardening behavior of the bulk and the GBs, obtaining different predictions of the local fields and overall behavior, as a function of grain size. Even if in these calculations the GB thickness were overestimated (tens of nanometers) compared to the value of ~1nm suggested by Molecular Dynamics (MD) simulations [21], its importance resides in suggesting the way of dealing with the complex microstructure of nanocrystalline materials, i.e. modeling the material as an aggregate of single crystal cores surrounded by outer layers of GB regions with different constitutive responses.

Jiang and Weng [11] proposed a generalized elastoplastic self-consistent (SC) formulation, based on Christensen and Lo's [22] solution of the concentric double inclusion problem, extending from polycrystals to aggregates with nano-sized grains the

classic elastoplastic SC formulation based on Eshelby's single inclusion problem. As expected, the generalized double inclusion model tends to the classic SC model when the GB thickness becomes negligible (coarse-grained case). In their generalized SC model, Jiang and Weng assumed: a) rate-independent crystal plasticity for grain interiors; b) an isotropic and pressure-dependent Druker's type yield condition [23] at GBs; and c) a physical length-scale, given by the dimension of the GB thickness, taken to be 1 nm. This generalized SC formulation was in turn used to study the grain size dependence in the nanometer range of the stress-strain response (initial yielding and hardening) of nanocrystalline Cu. Concerning the pressure dependence of this mechanical response (which is present in the local constitutive description of GBs and therefore should also affect the macro behavior via the proposed homogenization theory), it was not investigated further in Jiang and Weng's paper. Finally, it should be mention that, given its rate-insensitive character, strain-rate effects cannot be considered using Jiang and Weng's approach.

In a recent contribution, Bringa et al. [24] interpreted the stress profiles obtained by MD simulations of shocks in nanocrystalline Cu in terms of different shock pressure dependences of slip and GB accommodation. These authors assumed a linear dependence with shock pressure of the flow stresses behind the shock front associated with both dislocation slip (i.e. Steinberg-Guinan model for shock-induced dislocation plasticity [18]), and GB accommodation (inspired in Mohr-Coulomb's law for plasticity of amorphous materials [9,10]). Adjusting the corresponding pre-factors using MD results, they proposed that the yield strength is given by the minimum between the flow stresses associated with dislocation slip and GB accommodation. Both mechanisms depended on grain size and applied pressure. This simple approach proved to be compatible with the reported Cu MD results and Ni experiments, suggesting that, due to the apparent suppression of the softening associated with GB accommodation, the flow stress can reach ultrahigh values, at the high pressures produced by shock-loading. However, as it was already acknowledged in [24], the use of a simple minimum criterion to decide whether the macroscopic yield strength is equal to the flow stress associated with either

slip or GB accommodation, does not consider the likely occurrence of strain partition between both mechanisms.

Based on some of the assumptions and ideas from these earlier models, in this work we report a new micromechanical formulation to study the effect of grain size, pressure and strain rate on the yield strength of fcc nanocrystalline materials. The proposed model is a full-field approximation that takes into account the actual topology of the aggregate consisting in bulk crystalline regions surrounded by a GB percolating phase. Both regions co-deform plastically according the following constitutive behaviors: a) for grain interiors: crystal viscoplasticity, with Hall-Petch grain size dependence, and in the case of shocks, Steinberg-Guinan pressure dependence of the flow stress for slip activation; b) for grain boundaries: isotropic viscoplasticity with flow stress independent of grain size, and Mohr-Coulomb pressure dependence. The rate dependence of the proposed model can be kept in terms of the power laws representing the behaviors of both regions, or eliminated using an appropriate normalization. If the rate dependence is kept, rate effects under quasiestatic loading conditions also can be taken into account. The length-scale of the problem is given by the GB thickness, taken to be 1 nm. Instead of using Finite Element analysis as in [19,20], we use here a very efficient approach based on the Fast Fourier Transform (FFT) algorithm. This FFT-based solution of a unit cell problem for a representative volume element (RVE) gives the local mechanical fields that develop inside heterogeneous materials in great detail [25-28]. Periodic boundary conditions, required for this type of spectral approximation, are sufficient for the kind of parametric study that we want to perform. It is worth noting that, given the viscoplastic character of the present approach, it is not intended to describe elastic effects. In particular, in the case of shock-loading, no attempt is made here to develop a micromechanical modeling of the complex problem of propagation of elastoplastic waves in shocked materials (e.g. [29]). Instead, the present model aims at considering the yield strength resulting from the microstructural changes left in the material after the passage of a shock front.

The plan of the paper is as follows: in section 2 we briefly review the FFT-based model and discuss the construction of self-similar RVEs that represent nanostructured

polycrystals having the same topology and crystallographic texture, differing only in grain size. Next, we address the way of tackling rate effects with the present approach, and introduce the grain size and pressure dependences of our constitutive representation. In section 3 we present and discuss the local fields predicted by the model and show results on the pressure-dependent behavior of nanocrystalline copper after shock-loading, using constitutive parameters derived from Molecular Dynamics simulations and experiments [24]. Next, the proposed model is used to study the increased strain-rate sensitivity of nanostructured materials under quasiestatic loading conditions. In section 4 we draw conclusions from this work and mention potential applications of the proposed micromechanical approach.

2- MODEL

Suquet and coworkers [25-27] developed an iterative method based on FFT to compute effective properties and local fields of heterogeneous materials. In turn, Lebensohn and coworkers [28, 30-31] adapted this FFT-based formulation to compute local fields and texture development of viscoplastic anisotropic polycrystals. The FFT-based formulation delivers a full-field solution, i.e. the values adopted by the micromechanical fields in every point of a regular grid that covers the space, of the equilibrium and compatibility differential equations. It is in general faster than a Finite Element calculation for the same purpose and resolution, however limited to periodic boundary conditions. It shares some common characteristics with the Phase-Field method, although it is limited to what in Phase-Field jargon is known as long-range interactions (e.g. see [32]), since no heterogeneous chemical energy term is needed when solving a single-phase polycrystal. Recently, a similar kind of Phase-Field analysis was proposed [33] to obtain the local fields in elastically heterogeneous polycrystals. The FFT-based approach, however, is not restricted to linear behaviors. Problems involving non-linear heterogeneous materials (e.g. viscoplastic polycrystals) are treated similarly to a linear problem, using the concept of linear comparison material (e.g. [34]).

2-1 Construction of RVEs and discretization

The FFT-based formulation is based on the solution of a unit cell problem for a RVE with periodic boundary conditions. In the present case, the unit cell represents an aggregate of single crystal grains with prescribed orientations, surrounded by outer layers of percolating grain boundary regions. The particular orientation of each single crystal determines different anisotropic plastic properties from grain to grain, while, due to its intrinsic disordered character, the GBs are assumed to have a homogeneous isotropic behavior throughout the interconnected "GB phase". A 3-D implementation of the FFT-based method requires to discretize a cubic unit cell using a regular grid of NxNxN Fourier points (FPs). In this work we adopted N=128, resulting in 2097152 discretization points. Each FP belongs either to a grain interior, or to the GB phase. The dimensions of such Fourier grid are large enough such that each grain and the GB phase are represented by a large number of Fourier points. The length-scale associated with the RVE is determined by the GB thickness, taken to be 1 nm. In order to study the effect of grain size without interference of other microstructural characteristics (like crystallographic texture, or any particular orientation correlation between neighbour grains) self-similar RVEs were generated as follows. First, the 3-D unit cell was partitioned into grains by Voronoi tessellation. Given that a FFT-based calculation requires a discrete mapping of the microstructure on a regularly-spaced grid, this procedure is simpler than determining the exact position of the boundaries between Voronoi cells in a continuum. This discrete Voronoi procedure consists in randomly distributing 27 grain nuclei (with random crystallographic orientations) in the cubic unit cell and assigning each FP to its nearest nucleus, accounting for periodic boundary conditions across the RVE limits. Next, in order to determine the FPs belonging to the GB phase, the sets of Fourier points with up to first, second and third neighbours belonging to a different grain were identified. A fourth set was obtained by choosing one of the two points of each pair of first-neighbour FPs belonging to different grains. Next, by assigning these four sets of Fourier points to the GB phase, four self-similar RVE were determined, with the same number of grains and the same topology and crystallographic texture, differing only in the volume fraction

of GB phase. If in all cases the GB thickness is taken to be 1 nm, a simple formula involving the volume fraction of GB phase gives the average grain size of the RVE:

$$d = \frac{1\,\text{nm}}{1-(1-x_{GB})^{1/3}} \tag{1}$$

Table 1 reports the resulting GB volume fractions and grain sizes of the four RVEs used in this work. Figure 1 shows four 2-D sections (YZ cuts at X=64) corresponding to the four RVEs. The GB regions are represented in white. Regarding the grains, for later analysis, the gray shades represent the relative yield strength of each grain under uniaxial tension or compression, i.e. lighter (darker) shades represent softer (harder) grains.

2-2 Local constitutive behavior

The local constitutive equation for a point $\mathbf{x}$ belonging to a grain interior is given by the following power law for single crystal viscoplasticity [35]:

$$\begin{aligned}\dot{\boldsymbol{\varepsilon}}(\mathbf{x}) = \sum_s \boldsymbol{\mu}^s(\mathbf{x})\,\dot{\gamma}^s(\mathbf{x}) = \dot{\gamma}_o \sum_s \boldsymbol{\mu}^s(\mathbf{x}) \left(\frac{\left|\tau^s(\mathbf{x})\right|}{\tau_o^s} \right)^{n_{GI}} \times \text{sign}\,\tau^s(\mathbf{x}) = \\ = \dot{\gamma}_o \sum_s \boldsymbol{\mu}^s(\mathbf{x}) \left(\frac{\left|\boldsymbol{\mu}^s(\mathbf{x}) : \boldsymbol{\sigma}(\mathbf{x})\right|}{\tau_o^s} \right)^{n_{GI}} \times \text{sign}\left[\boldsymbol{\mu}^s(\mathbf{x}) : \boldsymbol{\sigma}(\mathbf{x})\right]\end{aligned} \tag{2}$$

where $\dot{\boldsymbol{\varepsilon}}(\mathbf{x})$ and $\boldsymbol{\sigma}(\mathbf{x})$ are the local strain rate and stress tensors; $\boldsymbol{\mu}^s(\mathbf{x})$, $\dot{\gamma}^s(\mathbf{x})$, $\tau^s(\mathbf{x})$ and τ_o^s are, respectively, the orientation-dependent Schmid tensor, the shear rate, the resolved shear stress, and a reference shear stress, of slip system (s). The pre-factor $\dot{\gamma}_o$ is a reference shear rate, and n_{GI} is an exponent, which in an explicit rate-sensitive context can be associated with the inverse of the rate-sensitivity of the coarse-grained material (see section 2-4). Equation (2) expresses that the deformation rate is given by the sum over the shear rates contributed by all the 12 slip systems of the fcc crystal structure.

The local constitutive behavior for a point $\mathbf{x}$ belonging GB phase is here assumed to be given by the following J_2- isotropic power law for nonlinear isotropic materials [34]:

$$\dot{\boldsymbol{\varepsilon}}(\mathbf{x}) = \frac{3\dot{\varepsilon}_o}{2\sigma_{eq}(\mathbf{x})}\left(\frac{\sigma_{eq}(\mathbf{x})}{\sigma_o}\right)^{n_{GB}} \boldsymbol{\sigma}(\mathbf{x}) \tag{3}$$

where $\sigma_{eq}(\mathbf{x})$ and σ_o are the von Mises equivalent of the stress and a reference equivalent stress, respectively, $\dot{\varepsilon}_o$ is a reference strain rate, and n_{GB} is an exponent, which in a explicit rate-sensitive context can be identified as the inverse of the rate-sensitivity associated with the deformation mechanisms of GB accommodation.

2-3 FFT-based algorithm

The discretization described in section 2-1 determines a regular grid in the Cartesian space $\{\mathbf{x}_d\}$ and a corresponding grid in the Fourier space $\{\boldsymbol{\xi}_d\}$. The method requires the selection of a linear reference medium of stiffness $\mathbf{L}$ to convert a (periodic) heterogeneity problem into a homogeneous problem with polarization. Combining the latter with the equilibrium condition we obtain:

$$L_{ijkl}\, \dot{u}_{k,lj}(\mathbf{x}) + \chi_{ij,j}(\mathbf{x}) = 0 \tag{4}$$

where $\dot{u}_k(\mathbf{x})$ and $\chi_{ij}(\mathbf{x})$ are the periodic velocity and polarization fields. The resolution of Eq. (4) by Green functions requires considering the following auxiliary problem:

$$L_{ijkl}\, G_{km,lj}(\mathbf{x}-\mathbf{x}') + \delta_{im}\, \delta(\mathbf{x}-\mathbf{x}') = 0 \tag{5}$$

where $G_{km}(\mathbf{x})$ is the periodic Green function associated with the velocity field, and $\delta(\mathbf{x})$ is Dirac's delta. From Eq. (5), the Fourier transform of the symmetric Green operator $\hat{\boldsymbol{\Gamma}}(\boldsymbol{\xi}_\mathbf{d})$ associated with the periodic strain-rate field $\left(\dot{u}_{k,l} + \dot{u}_{l,k}\right)/2$ can be readily obtained for each point of grid in Fourier space (e.g. [28]). The FFT-based algorithm consists in finding a strain-rate field, associated with a kinematically admissible velocity field that minimizes the average of the local strain energies, under the constraint imposed by the strain compatibility condition. If a macroscopic strain rate $\dot{\mathbf{E}}$ is imposed on the

unit cell, the algorithm is initialized under a uniform strain rate assumption $\tilde{\dot{\boldsymbol{\varepsilon}}}^{0}(\mathbf{x}_d)=0$, where the symbol "~" denotes local deviation with respect to average. The corresponding initial guess of the stress field $\boldsymbol{\sigma}^{0}(\mathbf{x}_d)$ can be readily obtained inverting the local constitutive relations for grain interiors and grain boundaries, Eqs (2-3). Further, assuming $\boldsymbol{\lambda}^{0}(\mathbf{x}_d)=\boldsymbol{\sigma}^{0}(\mathbf{x}_d)$, where $\boldsymbol{\lambda}^{0}(\mathbf{x}_d)$ is the initial guess for a field of Lagrange multipliers associated with the compatibility constraint, the following iterative procedure can be started. If $\tilde{\dot{\boldsymbol{\varepsilon}}}^{i}(\mathbf{x}_d)$ and $\boldsymbol{\lambda}^{i}(\mathbf{x}_d)$ are known, the (i+1)th iteration starts with the calculation of the new guess of the polarization field:

$$\boldsymbol{\chi}^{i+1}(\mathbf{x}_d)=\boldsymbol{\lambda}^{i}(\mathbf{x}_d)-\mathbf{L}:\tilde{\dot{\boldsymbol{\varepsilon}}}^{i}(\mathbf{x}_d) \tag{6}$$

The Fourier transform of this polarization field results from:

$$\hat{\boldsymbol{\chi}}^{i+1}(\boldsymbol{\xi}_d)=\mathrm{fft}\left\{\boldsymbol{\chi}^{i+1}(\mathbf{x}_d)\right\} \tag{7}$$

where *fft* denotes the application of the (discrete) FFT algorithm. The new guess for the kinematically admissible strain rate deviation field in Fourier space can be then obtained as [27]:

$$\hat{\tilde{\dot{\boldsymbol{\zeta}}}}^{i+1}(\boldsymbol{\xi}_d)=-\hat{\boldsymbol{\Gamma}}(\boldsymbol{\xi}_d):\hat{\boldsymbol{\chi}}^{i+1}(\boldsymbol{\xi}_d),\ \forall\boldsymbol{\xi}_d\neq 0 \text{ and } \hat{\tilde{\dot{\boldsymbol{\zeta}}}}^{i+1}(0)=0 \tag{8}$$

After applying the inverse FFT to get $\tilde{\dot{\boldsymbol{\zeta}}}^{i+1}(\mathbf{x}_d)$, the new guess for the stress field is calculated from:

$$\boldsymbol{\sigma}^{i+1}(\mathbf{x}_d)+\mathbf{L}:\boldsymbol{\varepsilon}^{i+1}(\mathbf{x}_d)=\boldsymbol{\lambda}^{i}(\mathbf{x}_d)+\mathbf{L}:\left\{\dot{\mathbf{E}}+\tilde{\dot{\boldsymbol{\zeta}}}^{i+1}(\mathbf{x}_d)\right\} \tag{9}$$

where $\boldsymbol{\varepsilon}^{i+1}(\mathbf{x}_d)$ is related to $\boldsymbol{\sigma}^{i+1}(\mathbf{x}_d)$ through the local constitutive relations (Eqs. 2-3). The iteration is completed by calculating the new guess for the Lagrange multiplier field [27]:

$$\boldsymbol{\lambda}^{i+1}(\mathbf{x}_d)=\boldsymbol{\lambda}^{i}(\mathbf{x}_d)+\mathbf{L}:\left\{\tilde{\dot{\boldsymbol{\zeta}}}^{i+1}(\mathbf{x}_d)-\tilde{\dot{\boldsymbol{\varepsilon}}}^{i+1}(\mathbf{x}_d)\right\} \tag{10}$$

Convergence is reached when the corresponding strain rate deviation fields $\tilde{\dot{\boldsymbol{\varepsilon}}}(\mathbf{x}_d)$ and $\tilde{\dot{\boldsymbol{\xi}}}(\mathbf{x}_d)$, and stress fields $\boldsymbol{\sigma}(\mathbf{x}_d)$ and $\boldsymbol{\lambda}(\mathbf{x}_d)$, coincide within certain tolerance. With the converged solution, the values of stress, velocity gradient (strain rate and rotation rate) and velocity in each Fourier point can be obtained [28]. This allows us to compute the effective stress and strain rate in the polycrystal by averaging the corresponding local magnitudes over the entire unit cell, and to predict texture development, microstructure evolution and strain-hardening, as well [28].

2-4 Rate dependence

Two interpretations of the power law constitutive expressions (Eqs. 2-3) are possible. In grain interiors, under quasiestatic loading conditions, the physics of dislocation glide limited by discrete obstacles determines an Arrhenius relationship between the flow shear stress and the shear rate [36,37]:

$$\dot{\gamma}^s = \dot{\gamma}^o \exp\left\{-\frac{\Delta F}{kT}\left(1-\frac{\tau^s}{\tau_o^s}\right)\right\} \tag{11}$$

where ΔF is the total free energy required to overcome an obstacle without aid of external stress. ΔF is in general large, and this rate equation can be approximated by the expression:

$$\dot{\gamma}^s = \dot{\gamma}^o \left(\frac{\tau^s}{\tau_o^s}\right)^{n_{GI}} \tag{12}$$

used in Eq. (2). The microscopic rate sensitivity is defined as:

$$m^s = \left(\frac{\partial \ln \tau^s}{\partial \ln \dot{\gamma}^s}\right)_{T,\tau_o^s} = \frac{1}{n_{GI}} \tag{13}$$

Making the plausible assumption that $m^s = m_{CG}$ [38] (with m_{CG} being the macroscopic rate sensitivity of the coarse-grained material), the exponent of the power law for grains interiors (Eq. 2) has an actual physical meaning, i.e.

$$n_{GI} = \frac{1}{m_{CG}} \tag{14}$$

As for the constitutive relation for GBs (Eq. 3), the following assumption:

$$n_{GB} = 1 \tag{15}$$

represents the actual linear rate dependence associated with GB diffusional flow [37]. Therefore, if the power law exponents of Eqs. (2-3) are chosen according to expressions (14-15), i.e. giving them a meaning based on the actual physical mechanisms controlling deformation in the bulk of the grains and in GBs, the present formulation can be explicitly used to study the rate dependence of nanostructured materials.

When Eqs. (2-3) are used in a shock-loading context, the references stresses τ_o^s and σ_o should be interpreted as the variables that describe the plastic state in grain interiors and GBs, respectively, behind the shock front. In other words, the shock induces microstructural changes that result in a harder material after the passage of the shock [24]. In such case, the functional forms of the rate equations (2-3) cannot be interpreted in terms of actual microscopic deformation mechanisms. Therefore, a different interpretation should be given to them. For this, we use similar arguments as those given by Kok et al [39] in the context of a crystal plasticity-based Finite Element analysis of a coarse-grained polycrystalline material. These authors proposed a modification of the standard power law (Eq. 2) to eliminate any explicit strain-rate dependence associated with it. This was done in the context of the development of a slip version of the so-called Mechanical Threshold Stress (MTS) model [40]. The original MTS model is an isotropic scalar model that gives the macroscopic flow stress as a function of strain rate, temperature and current state through a state variable called mechanical threshold. The slip version of the MTS model consists in assigning a threshold shear stress to each slip system. In order to eliminate the rate dependence from the power law equation, Kok et al [39] set the reference shear rate $\dot{\gamma}^o$ equal to the current macroscopic equivalent strain rate, i.e.

$$\dot{\gamma}_o = \dot{E}_{eq} = \sqrt{\frac{2}{3}\dot{\mathbf{E}} : \dot{\mathbf{E}}} \tag{16}$$

In this way, the power law (Eq. 2) is retained for mathematical convenience, but the local stress remains unchanged as the strain rate changes. In the present formulation, for consistency, the reference strain rate associated with GB accommodation (see Eq. 3) should also be chosen as $\dot{\varepsilon}_o = \dot{E}_{eq}$. Then, the exponents involved in Eqs. (2-3) are set equal to a convenient value, e.g.:

$$n_{GI} = n_{GB} = 20 \tag{17}$$

In this way, any sensitivity (e.g. to strain rate, temperature, grain size or pressure) of the proposed constitutive description, if known, should be given by the functional dependence of τ_o^s and σ_o with the above variables. In the following section we describe the pressure and grain size dependence adopted in this work.

2-5 Pressure and grain size dependence

Concerning the explicit pressure and grain size dependence of our state variables we adopted Bringa et al. [24] approach, with slight modifications. Based on preexisting models (Steinberg-Guinan and Hall-Petch), these authors proposed the following dependences with shock pressure and grain size for the flow stresses behind a shock front, associated with dislocation glide in grain interiors and deformation accommodation at grain boundaries, respectively:

$$\sigma_{GI} = C\left(G_o + \beta P\right)\left(d/d_o\right)^{-0.5} \tag{18a}$$

$$\sigma_{GB} = \left(\sigma_a + \alpha P\right)\left(1 + d/d_o\right) \tag{18b}$$

where P is the shock pressure, G_o is the shear modulus at zero pressure, C is material-dependent adjustable parameter, σ_a is the flow stress of the amorphous material at zero pressure, α and β are pressure-sensitivity factors, and d_o is a reference grain size. Here, we adopt:

$$\tau_o^s = \frac{C\left(G_o + \beta P\right)\left(d/d_o\right)^{-0.5}}{\overline{M}_{CG}} \tag{19a}$$

$$\sigma_o = \sigma_a + \alpha P \tag{19b}$$

i.e. we have introduced two modifications: a) in Eq. (19a), a factor $1/\overline{M}_{CG}$ was added. $\overline{M}_{CG}$ is the average Taylor factor (i.e. the ratio between the effective stress and the reference slip stress) of the untextured coarse-grained material, whose local constitutive equation is given by Eq. (2). $\overline{M}_{CG}$ is model-dependent and also depends on the applied strain-path and the exponent in Eq. (2) (e.g. for uniaxial tension or compression and an exponent of 50, the FFT-based model gives $\overline{M}_{CG} = 2.28$); b) the grain size dependence disappeared from Eq (19b). Provided the volume fraction of GBs is explicitly accounted for in the present model, it turns out to be unnecessary to include a grain size dependence in the constitutive law for GB accommodation, as it was proposed in [41], using scaling arguments within the context of a simple phenomenological model.

For the choice of the parameters involved in Eqs. (19), we followed Bringa et al [24] and references therein. The value of σ_a has been estimated to be 0.9 GPa for Cu [42]. Using MD, these authors calculated the elastic constants for Cu as a function of pressure (at T=0K), obtaining $G_o = 45\text{GPa}$, and $\beta \approx 1$ for P<60 MPa, in agreement with experiments [43]. The value of the pressure-sensitivity factor for GB accommodation α was assumed to be $\alpha = 0.04$, i.e. within the range reported in Ref. [9] from energy minimization calculations in amorphous metals. The adopted reference grain size was $d_o = 30\text{ nm}$ and, by assuming that the flow stresses of slip and GB accommodation are equal when the grain size is d_o, a value of C=0.04 was obtained. It should be also mentioned that the values of the relevant model parameters given above were also adopted to simulate deformation under quasiestatic conditions (see sections 3-1 and 3-3), by setting the shock pressure to zero in Eqs. (19).

3- RESULTS

3-1 Grain size dependence of local deformation fields

Figure 2 shows the 2-D section maps of local von Mises equivalent strains for the four self-similar RVEs, relative to the applied macroscopic von Mises equivalent strain, for the case of nanocrystalline Cu deformed in quasiestatic (P=0 in Eqs 19) axisymmetric compression along the z-axis. The 2-D sections shown in Fig. 2 correspond to the same YZ cuts as the ones displayed in Fig 1 (note that the compression axis lies in the vertical direction). The main observation is that the strain is concentrated at GBs, reaching 10 times the macroscopic strain, while significant portions of the grain interiors undergo local strains which are less than the applied macrostrain. This trend is more marked as grain size decreases, e.g. see the center grain (marked "A"). Another interesting observation is that the grains that deform the most (e.g. grain "A") are not necessarily the softest (e.g. grain "A" has an intermediate yield strength, see Fig. 1) but the most ubiquitous. For instance, in the 29 and 15 nm cases, grain "A" provides a link between GBs well oriented for the propagation of a transgranular deformation band at approximately 50 degrees with respect to the compression direction. At smaller grain sizes, the fine structure of the strain field can be observed inside the GBs. Interestingly, the strain seems to concentrate near the transition zones between GB and the bulk of the grains, especially near triple junctions. This may indicate the occurrence of local shears consistent with grain boundary sliding and grain rotation.

Fig. 3 shows the relative activities (strain partition) in the grain interiors and the GB phase, along with the corresponding volume fractions, as a function of grain size, corresponding to the cases shown in Fig. 2. The relative activities are defined as local strains averaged over all of the Fourier points belonging to each region, normalized by the macroscopic strain. Consistent with the results of Fig. 2, the relative activity at GB exceeds the corresponding GB volume fraction. This trend is more marked as the grain size decreases. At 5 nm, the grain interiors contribute only with 10% to the overall strain, while they still represent almost half of the volume. This result is consistent with most of

the reported MD simulations at these grain sizes [5], although we note that MD has not yet given a quantitative measurement as presented in Fig. 3.

3-2 Pressure dependence of yield strength under shock loading

Figure 4 shows the pressure and grain size dependence of the yield strength of nanostructured samples, as predicted by the present model, using the constitutive equations and parameters for Cu given by Eqs (2), (3), (16), (17) and (19), and described in section 2-4. The main characteristics of these curves are: a) as expected from the type of pressure dependence adopted for the local constitutive behaviors (Eqs 19), the yield stress increases with shock pressure, for all grain sizes, b) the Hall-Petch inversion is observed at around 10 nm for all pressures, c) the line joining the yield strength maxima exhibits a negative slope. This result is the outcome of the present model that considers a detailed partitioning of strain between GBs and grain interiors and is therefore to be compared with Fig. 1 of Ref. [24] in which a qualitative minimum criterion for the flow stress was used. From this comparison the differences in the location and the slope of the Hall-Petch inversion curves are apparent. In particular, the significant decrease of the Hall-Petch inversion point with increasing pressure reported in [24], which would maximize the yield strength under shock loading for smaller grain sizes as pressure increases, seems to be only marginal in the context of the present, more refined approach.

Figure 5 shows the effect of pressure on the strain partition between slip and GB accommodation (for sake of clarity, only the relative slip activity curves are shown, the GB relative activity can be obtained subtracting the slip activities from unity). As shock pressure increases, slip activity increases. The inserted figure shows in more detail the predictions for the smallest grain sizes. While for a grain size of 5 nm the slip activity at 22 GPa shows about 50% increase with respect to the P=0 case, for larger grain sizes this relative increase is only marginal. Given that the dislocations are the carriers of plastic deformation inside the grains, the significant increase of slip activity at smaller grain sizes and higher pressures should involve a larger number of dislocations gliding through

the grains. Such increase in the number of dislocations as grain size decreases and shock pressure increases has also been found in MD simulations [24].

3-3 Strain-rate dependence of yield strength under quasiestatic loading

In this section we show results of the model for quasiestatic loading conditions. The rate dependence is considered to be explicitly related to the power law exponents of Eqs (2-3). We have adopted $n_{GI} = 50$ and $n_{GB} = 1$. This value of n_{GI} corresponds to a rate-sensitivity of the coarse-grained material $m_{CG} = 0.02$. The latter is compatible with warm deformation of fcc materials (e.g. m=0.025 for CG Al deformed at 250 ºC [13]). Figure 6a shows the yield strength variations in the strain rate range 10^{-2}-10^{0} s^{-1}, for axisymmetric compression, as predicted for the 15 nm RVE. For comparison, we have included the strain-rate dependence of the coarse-grained material (100 μm). The resulting effective strain-rate sensitivity of the 15 nm material is m=0.155 (representing roughly an eight-fold increase with respect to the CG value of 0.02). This increase is comparable with the seven-fold increase with respect to the coarse-grained rate-sensitivity value reported by Lu et al [17] for the case of Cu containing nano-sized twins of ~20 nm width, deformed at room temperature; and also with the ten-fold increase reported by May et al. [13] in ECAP-deformed Al with grain size of ~300 nm deformed at 250 ºC. However, it should be acknowledged that the conditions of both the above experiments are not strictly the same as in our simulations. In the case of Cu with nanometer twins, the specific orientation correlation across the coherent twin boundaries could determine a significant difference with respect to the uncorrelated GB regions assumed in our model. Moreover, Lu et al. observations correspond to room temperature, while our simulations are compatible with warm-temperature deformation. (We have attempted to run simulations using room-temperature rate-sensitivity values: m=0.005, i.e. $n_{GI} = 200$, but the FFT-based algorithm becomes instable at those very high exponents). In what concerns the ECAP Al measurements, the main difference with respect to our simulations is the grain size, cf. grain sizes of ~300 nm in the experiments versus 15 nm in our simulations. (Here, again, we had numerical difficulties to run

simulations with grain size larger than 30 nm, to be closer to the experiments. Since the length scale is fixed by the GB thickness, 1 nm, the sizes of the Fourier grids needed to reach larger grain sizes are beyond standard computational resources).

Regarding the relative strain activity in the bulk and the GB regions at different strain rates, shown in Fig. 6b, the activity of GB accommodation increases as the strain rate decreases, reaching values of 80% (i.e. four times the GB volume fraction, also shown in the figure). This behavior reflects the fact that at lower strain rates there is more time for GB diffusion mechanisms (represented by the exponent $n_{GB} = 1$) to contribute profusely to the overall deformation. Interestingly, this significant increase in GB activity at lower rates apparently does not involve changes in the effective rate-sensitivity (i.e. in Fig 6a, the $\log \sigma$ vs. $\log \dot{\varepsilon}$ plot in the 15 nm grain size case remains linear).

4- CONCLUSIONS

We have presented a micromechanical approach based on Fast Fourier Transforms to study the role played by dislocation glide and GB accommodation in determining the plastic behavior of nanostructured materials. By constructing self-similar RVEs and using constitutive parameters obtained from experiments or derived from atomistic simulations, we were able to study the effect of grain size, strain rate and pressure on the local and effective behavior of fcc materials with nano-sized grains. In general, the local strain fields exhibit a strong concentration in GBs. In grain interiors, the strain is higher in grains which can serve as links between GB regions well-oriented with respect to the direction of maximum macroscopic shear, to form transgranular deformation bands.

Under shock-loading conditions, the qualitative pressure-sensitive model of Bringa et al. [24] was physically grounded by explicitly considering a material with two different constitutive behaviors, and by solving the strain partition between slip and GB activity. As expected from the type of pressure dependence adopted for the local constitutive behaviors, the predicted yield stress versus grain size curves are shifted upwards as the

shock pressure increases, while the predicted Hall-Petch inversion occurs (for the set of parameters adopted here) around 10 nm and shows a weak decrease with pressure. The relevance of these results appears clearly when we note that current constitutive models for shock-loading [18, 44] do not typically include grain size effects. These effects would be significant, for instance, for the design of the nanostructured targets under consideration for the National Ignition Facility [45].

At low strain rates, assuming a linear rate equation for GB accommodation (compatible with diffusion-driven mechanisms at GB), the model predicts a strain-rate sensitivity increase in materials with nano-sized grains with respect to coarse-grained, of the same order as in recently published experiments.

Further applications of the present model are worth considering. Although in this work we restricted our attention to the plastic response of nanostructured materials without microstructure evolution, the implementation of an incremental microstructure updating scheme is straightforward. For this, all the converged local rate fields can be assumed to be constant during a given time interval Δt, after which the current state of the material is updated. In particular, the resulting local rotation fields can be used to study the grain rotations associated with shear at grain boundaries. Also, the behavior of materials with special types of grain boundaries, like nanometer twin's boundaries, can be studied with the present approach.

Another appealing idea is to perform direct comparisons between the present continuum approach and MD simulations. For instance, in grain interiors, once the shear associated with slip system (s) at point **x** is obtained as $\dot{\gamma}^s(\mathbf{x})\Delta t$, the number of dislocations of s-type that have swept this point can be estimated as: $\dot{\gamma}^s(\mathbf{x})\Delta t \times d/b$, where b is the Burgers vector length. Hence, maps displaying the number and type of passed dislocations can be constructed for comparison with MD simulations for the same RVE.

Another feature of the plastic deformation of nanostructured materials scarcely investigated so far, which can be easily treated by means of the present approach, is anisotropy. The Severe Plastic Deformation (SPD) processing commonly used to obtain ultrafine-grained (UFG) materials usually results in samples with non-uniform morphologic and/or crystallographic textures (e.g. [13]). The influence of this anisotropic UFG microstructure can be readily studied with the present model by constructing unit cells having grains with orientations and shapes representative of the actual crystallographic and morphologic texture of these SPD materials.

Finally, it should be mentioned the potential use of the present mesoscopic constitutive approach to bridge scales, from atomistic to macroscopic levels, for a microstructure-sensitive prediction of the mechanical behavior of nanocrystalline materials. In such multiscale context, the lower scale formulations would provide a physically-based description of the microscopic deformation mechanisms, while the macroscopic solution of the mechanical problem would account for the applied boundary conditions. The strategy of passing information from one scale to the other could be by direct interrogation to the lower scale models (e.g. [46]), or by using the mesoscopic model to pre-adjust some kind of constitutive function to be used in turn at the macroscopic level (e.g. [47] in the case of texture-induced anisotropy).

REFERENCES

1- Hall EO. Proc Roy. Soc. London B 1951; 64: 474.
2- Petch NJ. J. Iron Steel Inst 1973; 25: 174.
3- Meyers MA, Chawla KK. Mechanical Behavior of Materials. Upper Saddle River, NJ: Prentice-Hall, 1999.
4- J.R Weertman. In: Koch CC, editor. Nanostructured Materials: Processing, Properties and Potential Applications. Norwich, NY: William Andrew, 2002, p.397.
5- Schiøtz J, Jacobsen KW. Science 2003; 301: 1357.
6- Van Swygenhoven H, Spaczer M, Caro A, Farkas D. Phys Rev B 1999; 60: 22.

7- Schiøtz J, Vegge T, Di Tolla FD, Jacobsen KW, Phys Rev B 1999; 60: 11971.
8- Kumar KS, Van Swygenhoven H, Suresh S, Acta Mater 2003; 51: 5743.
9- Schuh CA, Lund AC. Nat Mater 2003; 2: 449.
10- Lund AC, Schuh CA. Acta Mater 2005; 53: 3193.
11- Jiang B, Weng GJ. J Mech Phys Solids 2004; 52: 1125.
12- Wang YM, Ma E. Appl Phys Lett 2003; 83: 3165.
13- May J, Höppel HW, Göken M. Scripta Mater 2005; 53: 189.
14- Lu L, Li SX, Lu K. Scripta Mater 2001; 45: 1163.
15- Dalla Torre F, Van Swygenhoven H, Victoria M. Acta Mater 2002; 50: 3957.
16- Schwaiger R, Moser B, Dao M, Chollacoop N, Suresh S. Acta Mater 2003; 51: 5159.
17- Lu L, Schwainer R, Shan ZW, Dao M, Lu K, Suresh S. Acta Mater 2005; 53: 2169.
18- Steinberg DJ. J Appl Phys 1980; 51: 1498.
19- Fu HH, Benson DJ, Meyers ME. Acta Mater 2001; 49: 2567.
20- Fu HH, Benson DJ, Meyers ME. Acta Mater 2004; 52: 4413.
21- Caro A, Van Swygenhoven H. Phys Rev B 2001; 63: 134101.
22- Christensen RM, Lo KH. J Mech Phys Solids 1979; 27: 315.
23- Druker DC. Q Appl Math 1950; 7: 411.
24- Bringa EM, Caro A, Wang YM, Victoria M, McNaney JM, Remington BA, Smith RF, Torralva BR, Van Swygenhoven H, Science 2005; 309: 1838.
25-Moulinec H, Suquet P. C R Acad Sci Paris II 1994; 318: 1417.
26-Moulinec H, Suquet P. Comput Methods Appl Mech Eng 1998; 157: 69.
27-Michel JC, Moulinec H, Suquet P, Comput Model Eng Sci 1999; 1: 79.
28- Lebensohn RA, Acta mater 2001; 49: 2723.
29- Molinari A, Ravichandran G. J Appl Phys 2004; 95: 1718.
30- Lebensohn RA, Liu Y, Ponte Castaneda P. Proc R Soc Lond A 2004; 460: 1381.
31- Lebensohn RA, Liu Y, Ponte Castaneda P. Acta Mater 2004; 52: 5347.
32- Chen LQ. In: Raabe D, Roters F, Barlat F, Chen LQ editors. Continuum Scale Simulations of Engineering Materials: Fundamentals, Microstructures, Process Applications. Wenheim: Wiley, 2004, p.37.
33- Wang YU, Jin YMM, Khachaturyan AG,. J Appl Phys 2002; 92: 1351.
34- Ponte Castaneda P, Suquet P. Adv Appl Mech 1998; 34: 171.

35- Asaro RJ, Needleman A, Acta Metall 1985; 33: 923.

36- Kocks UF, Argon AS, Ashby MF. Prog Mat Sci 1975; 19: 1.

37- Frost HJ, Ashby MF. Deformation-Mechanisms Maps. Oxford, UK: Pergamon Press, 1982.

38- Hutchinson JW. Proc R Soc London A 1976; 348: 101.

39- Kok S, Beaudoin AJ, Tortorelli DA. Int J Plasticity 2002; 18: 715.

40- Follansbee PS, Kocks UF, Acta Metall 1988; 36: 81.

41- Van Swygenhoven H, Caro A. Phys Rev B 1998; 58: 11246.

42- Estrin Y, Hellmig RJ, Kim HS. J Metastable Nanocrystalline Mat 2003; 17: 29.

43- Landolt-Börnstein New Series Tables, Springer-Verlag, 1986.

44- Preston DL, Tonks DL, Wallace DC. Appl Phys 2003; 93: 212.

45- Dittrich, TR, Haan SW, Marinak MM, Hinkel DE, Pollaine SM, McEachern R, Cook RC, Roberts CC, Wilson DC, Bradley PA, Varnum WS. Laser Part Beams 1999; 17: 217.

46- Tomé CN, Maudlin PJ, Lebensohn RA, Kaschner GC. Acta Mater 2001; 49: 3085.

47- Plunkett B, Lebensohn RA, Cazacu O, Barlat F. Acta Mater, submitted.

This work was performed under the auspices of the U. S. Department of Energy by University of California, Lawrence Livermore National Laboratory under contract W-7405-Eng-48.

TABLE CAPTIONS

Table 1: Grain boundary volume fraction, grain size and construction criterion of the four self-similar RVEs used in this work.

FIGURE CAPTIONS

Figure 1: 2-D sections (YZ plane at X=64) of to the four self-similar 3-D RVEs. White regions: grain boundaries; grey regions: grains. Lighter (darker) shades represent softer (harder) grains under uniaxial tension or compression.

Figure 2: Predicted 2-D section maps (YZ plane at X=64) of local von Mises equivalent strains, relative to the applied macroscopic von Mises equivalent strain, for axisymmetric compression along the z-axis, with no superimposed hydrostatic pressure.

Figure 3: Strain and volume fraction partition as a function of grain size, for axisymmetric compression along the z-axis.

Figure 4: Predicted yield strength as a function of grain size for different shock pressures (in GPa). Constitutive parameter values for nanocrystalline Cu, after Bringa et al [24].

Figure 5: Predicted slip activity as a function of grain size for different shock pressures (in GPa). Constitutive parameter values for nanocrystalline Cu, after Bringa et al. [24].

Figure 6: a) Predicted log-log plot of yield strength vs. strain rate for axisymmetric compression (with no superimposed hydrostatic pressure) for the 15 nanometer-grain and the coarse-grained material. b) GB relative activity for the 15 nm case. GB volume fraction = 0.1918 also shown.

FPs assigned to GBs	GB volume fraction	Grain size
one point from every pair of first neighbours belonging to different grains	0.1007	29 nm
every point with first neighbours belonging to a different grain	0.1918	15 nm
every point with first or second neighbours belonging to a different grain	0.3588	7 nm
every point with first, second or third neighbours belonging to a different grain	0.5024	5 nm

Table 1

Self-similar Representative Volume Elements
YZ plane, X=64

29 nm

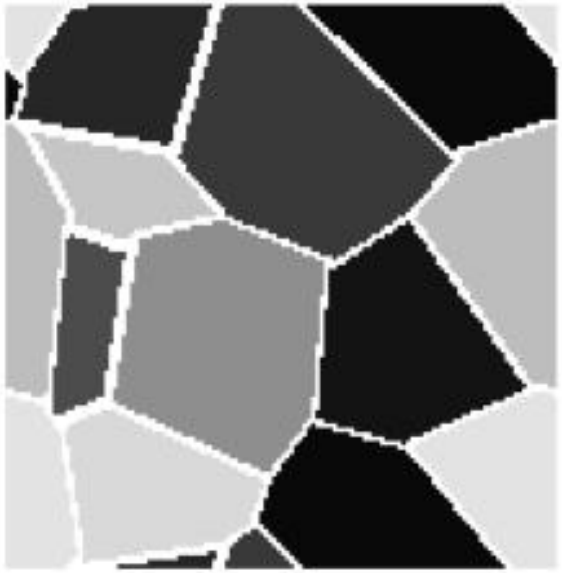

15 nm

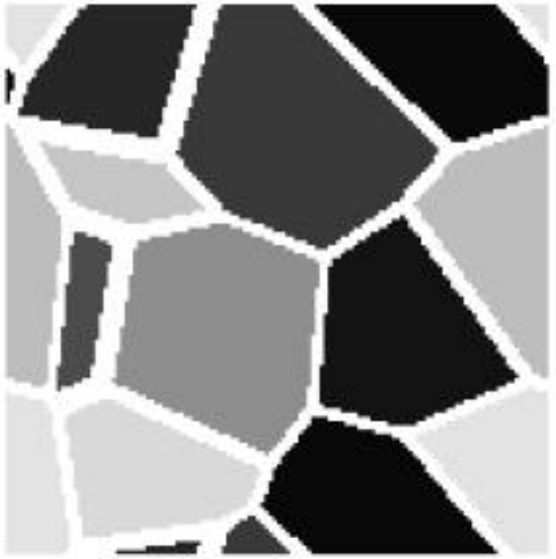

7 nm

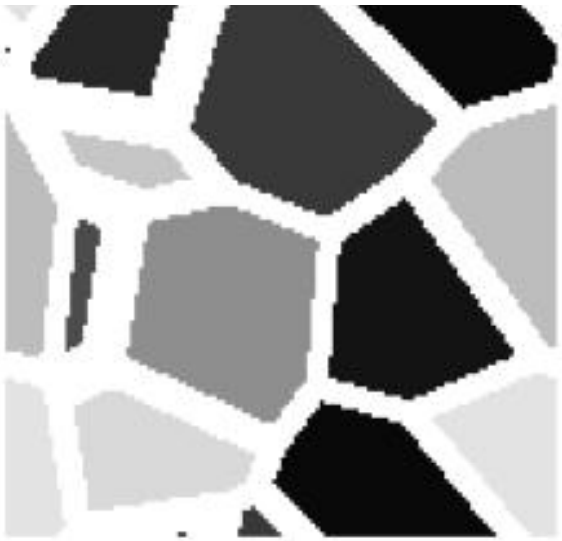

5 nm

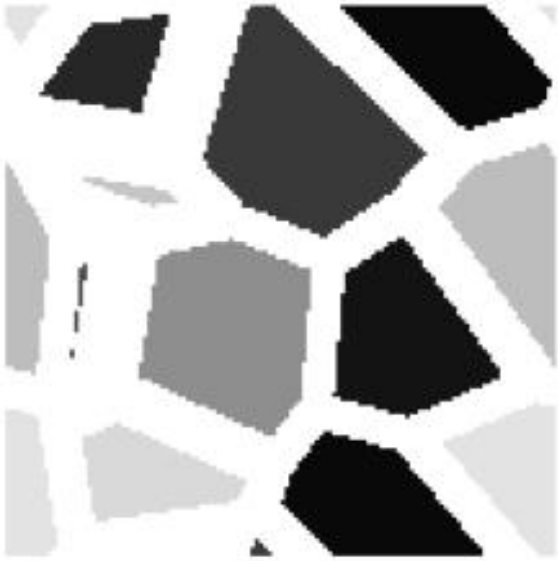

Fig. 1

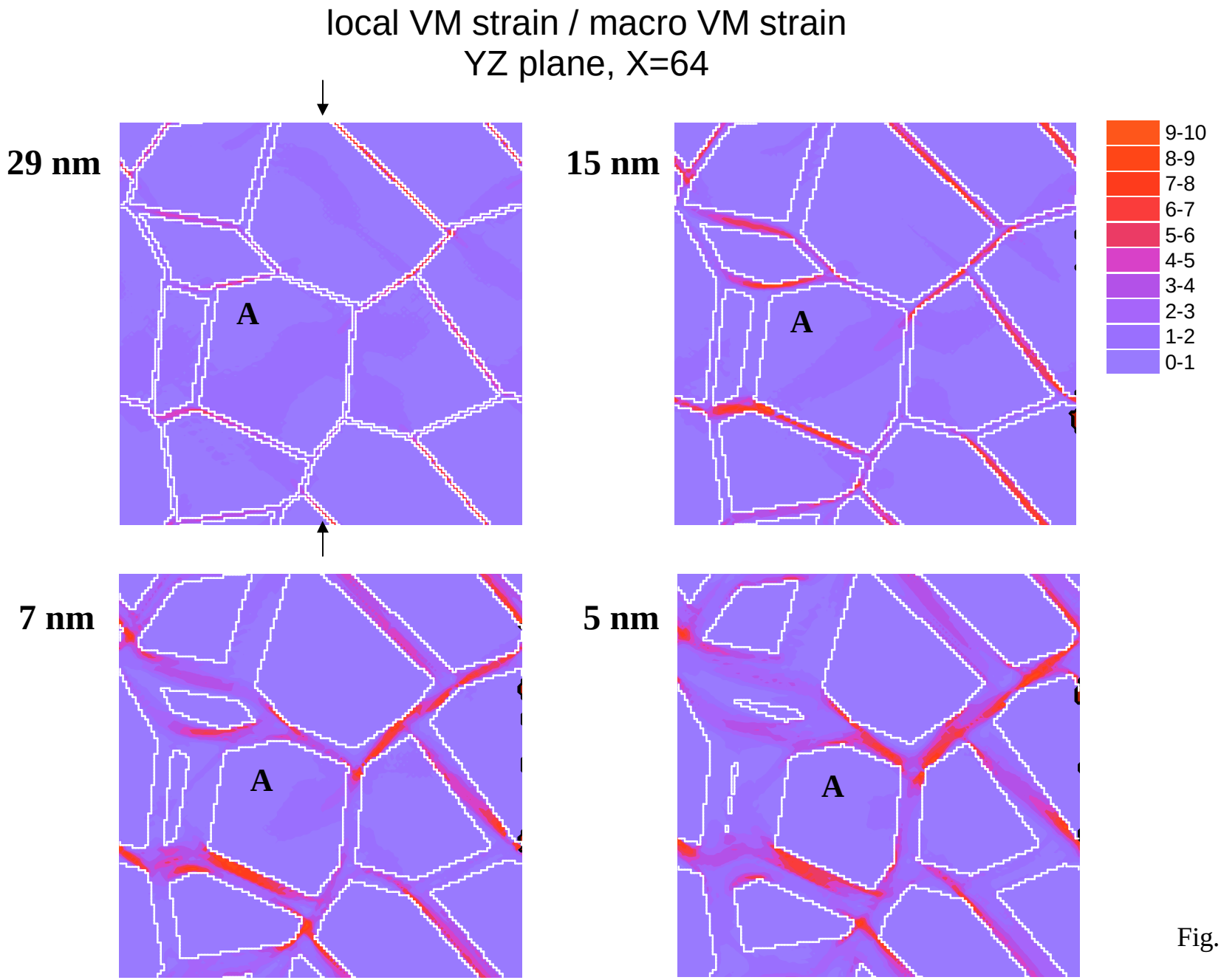
local VM strain / macro VM strain
YZ plane, X=64
29 nm
15 nm
7 nm
5 nm
A
A
A
A
9-10
8-9
7-8
6-7
5-6
4-5
3-4
2-3
1-2
0-1

Fig. 2

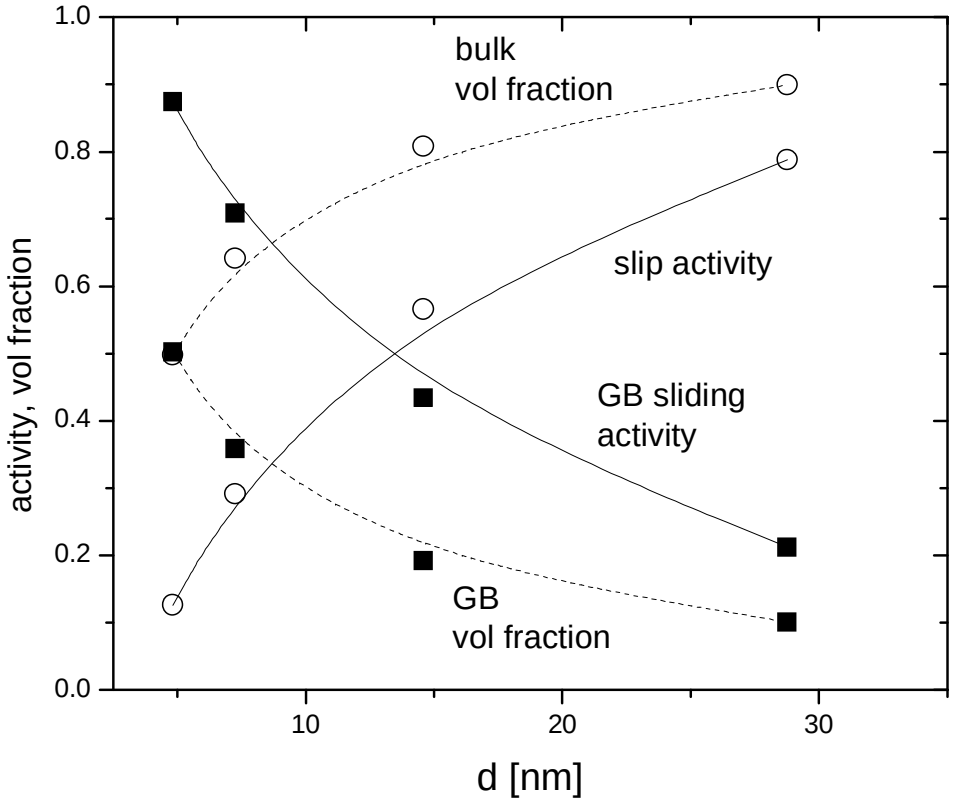
1.0
0.8
0.6
0.4
0.2
0.0
activity, vol fraction
10
20
30
d [nm]
bulk
vol fraction
slip activity
GB sliding
activity
GB
vol fraction

Fig. 3

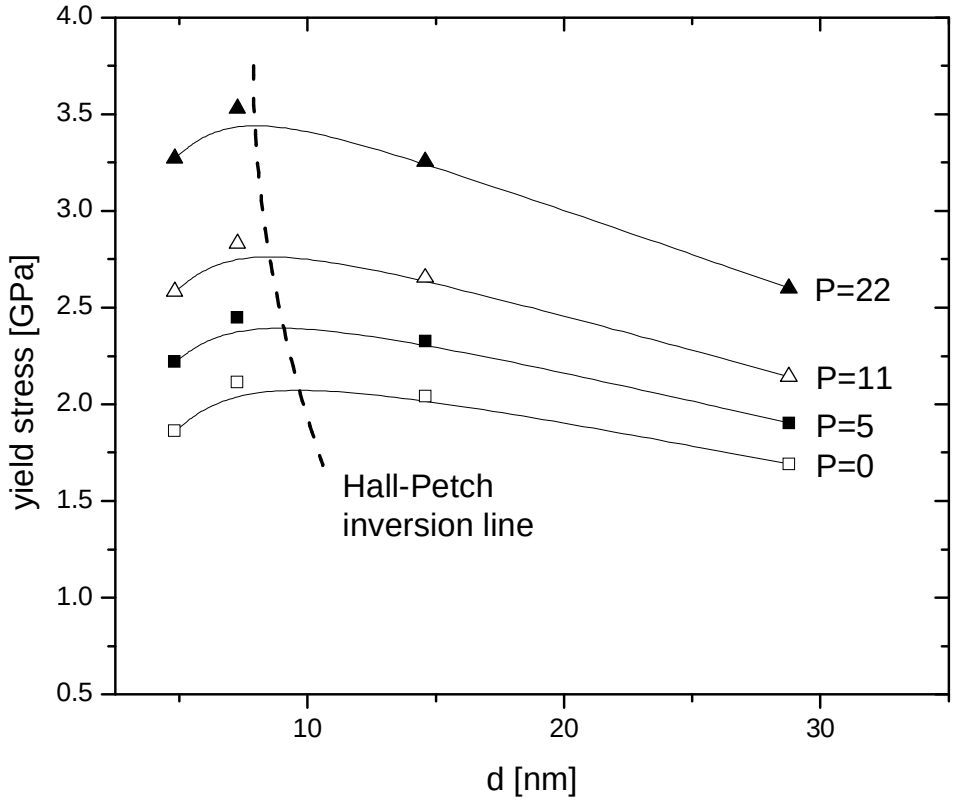
4.0
3.5
3.0
2.5
2.0
1.5
1.0
0.5
yield stress [GPa]
10
20
30
d [nm]
P=22
P=11
P=5
P=0
Hall-Petch
inversion line

Fig. 4

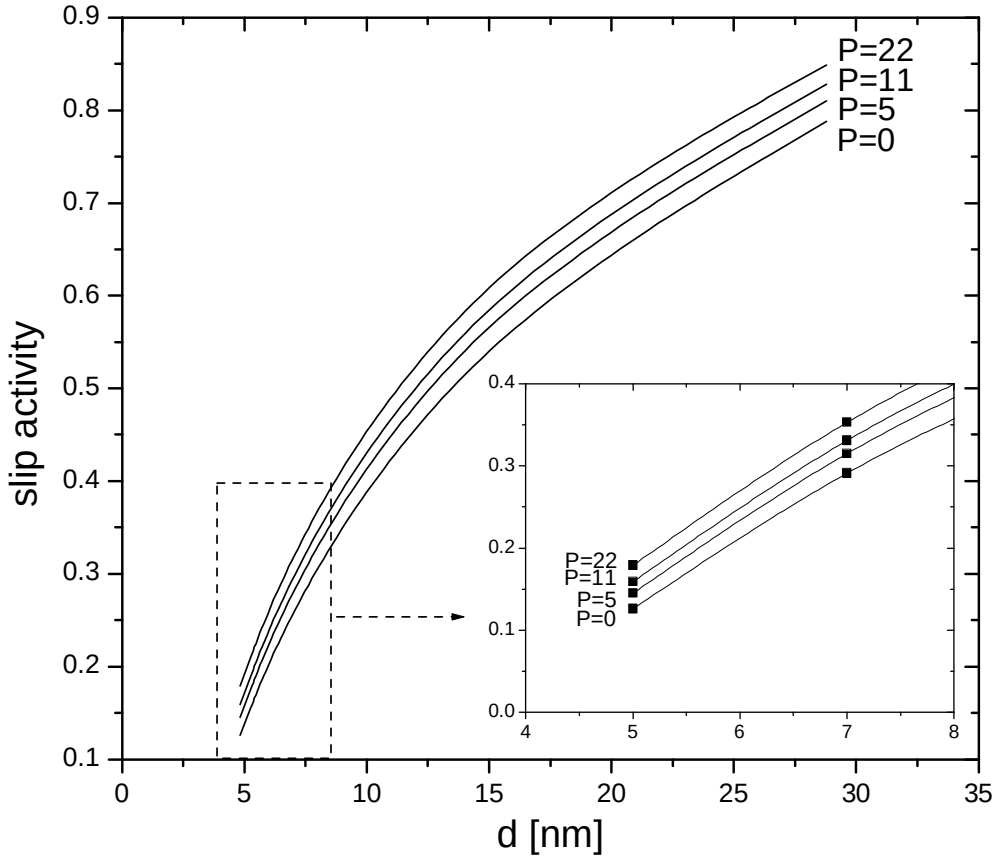
slip activity
d [nm]
P=22
P=11
P=5
P=0
0.9
0.8
0.7
0.6
0.5
0.4
0.3
0.2
0.1
0
5
10
15
20
25
30
35
0.4
0.3
0.2
0.1
0.0
4
5
6
7
8
P=22
P=11
P=5
P=0

Fig. 5

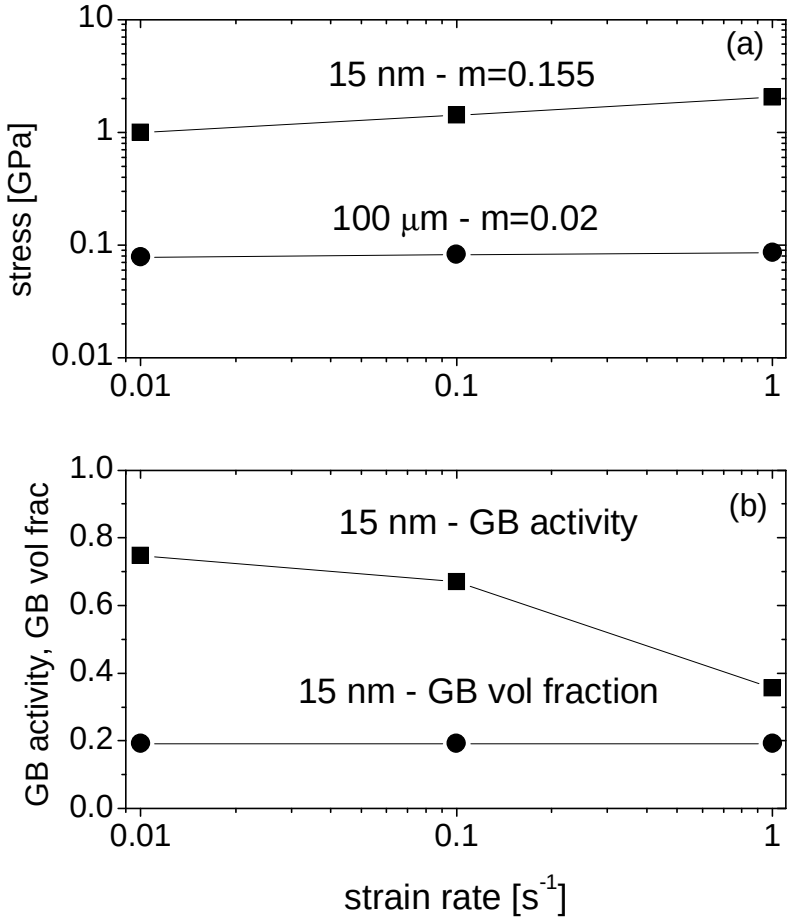
10
1
0.1
0.01
stress [GPa]
(a)
15 nm - m=0.155
100 μm - m=0.02
0.01
0.1
1
1.0
0.8
0.6
0.4
0.2
0.0
GB activity, GB vol frac
(b)
15 nm - GB activity
15 nm - GB vol fraction
0.01
0.1
1
strain rate [s-1]

Fig. 6